High Current Inductor Design for MHz Switching

M. Duffy*, C. Collins*, F. M. F. Rhen**, P. McCloskey**, S. Roy**
*Power and Energy Research Centre, NUI Galway, Ireland
**Tyndall National Institute, Cork, Ireland

Abstract— **High current inductor applications operating in the MHz range are generally limited to Voltage Regulator Modules (VRM's) and Point of Load (POL) power supplies, where the issue of fast transient response demands reduced inductance values. State-of-the-art controller IC's enable switching frequencies up to 8 MHz for low current POL applications. However, for current levels higher than 1 A, commercial inductors are not generally quoted as suitable for operation beyond 5 MHz. The application of electroplated metal alloy foils to produce competitive discrete cores suitable for operation in the range of 1 – 5 MHz is investigated in this paper.**

I. Introduction

Depending on the frequency of operation, high current inductor designs are limited either by saturation or by loss, with the latter being particularly true at high frequency. Indeed, in the MHz range, there is a lack of core materials with sufficiently low loss characteristics for application in VRM and POL inductors, for example. Thin film metal alloys have been proposed for high frequency power inductors in the past [1], where the possibility of depositing thin laminated layers provides the potential for overcoming eddy-current loss and low coercivity limits hysteresis loss. However, in most cases reported to date, low current inductor applications have been targeted for integration in silicon [2], [3]. Higher current levels were considered by the authors for CoNiFe layers integrated in PCB [4], where it was shown that measured loss properties are competitive to those of ferrite in the MHz range. In order to broaden the scope for application of the electroplated core materials, lower current POL applications are investigated in this paper. Furthermore, the application of the materials in discrete wound cores rather than integrated in PCB is investigated, so that the limited fill factor available with PCB can be overcome.

Applications for power converters switching in the MHz range are limited to point-of-load power supplies for computing loads, where conflicting requirements of high efficiency and fast transient response can be met. For high current VRM applications, the maximum frequency supported by controller IC's is typically 2 MHz [5], and this is also true of compatible inductor components [6]. The shift to higher frequency is seen in lower current POL applications [7–9], where the replacement of aluminium capacitors with ceramic chip capacitors provides significant reductions in circuit size. As a result, the inductor is often the largest component. The aim of this work is to demonstrate how electroplated alloys can address this by providing smaller solutions.

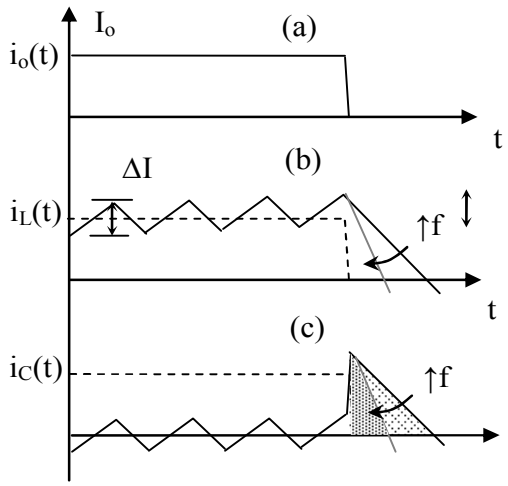

Fig. 1 POL waveforms (a) output current, $i_o(t)$, (b) inductor current, $i_L(t)$ and (c) capacitor current, $i_C(t)$

Point-of-load inductor specifications are reviewed in terms of commercial controller IC's and commercial inductor technologies in section II. Properties of electroplated alloy materials are presented in section III, where it is shown that the materials have lower losses, higher permeability and higher saturation flux density than available high frequency ferrite grades. In section IV, designs are presented for POL inductor beads, operating up to 5 MHz. Superior loss characteristics of the alloys result in structures that are up to 25% smaller than commercial inductors based on powdered metal cores and 54% smaller than can be provided with ferrite. Measurement results in section V demonstrate the application of the materials under typical DC/DC switching waveforms.

II. Point-of-Load Circuit Design

A. Commercial POL Controller IC's

Most commercial POL controller IC's are based on the simple buck converter, for which some operating waveforms are presented in Fig. 1. Within this, the function of the inductor, L, is to limit ripple current, ΔI, according to:

$$D(V_{in} - V_o) = fL\Delta I \quad (1)$$

and so as to provide reasonable efficiency, ΔI is generally limited to less than 50% of the output current, I_o. The initial choice of capacitance, C, is then determined by the allowed voltage ripple level, ΔV, as given by:

$$\Delta V = \frac{\Delta I}{8fC} + ESR.\Delta I + ESL\frac{\Delta I}{DT} \quad (2)$$

where steady-state ripple voltage is typically 1% of the output current [7]. The inclusion of the effects of equivalent series resistance (ESR) and equivalent series inductance (ESL) in (2) is particularly important for switching frequencies in the MHz range, where these parasitic impedances tend to dominate over pure capacitive impedance.

The choice of capacitance is then adapted to ensure voltage regulation during current transients. The worst case is shown in Fig. 1, where the current steps from its maximum value to zero at the end of the switch 'ON' time, and the inductor current discharge rate is limited to:

$$\frac{di_L}{dt} = \frac{V_o}{L} \quad (3)$$

With the load current changing at a much higher rate, the capacitor needs to sink the inductor current while maintaining voltage regulation to within ΔV_{trans} of the output value:

$$\Delta V_{trans} = \max\left\{ESR(I_o + \Delta I/2), \frac{L(I_o + \Delta I/2)^2}{2CV_o}\right\} \quad (4)$$

From (1), it is clear that the first advantage of increased switching frequency is that the inductance value required to limit ripple current is reduced, and this usually results in a physically smaller inductor. Secondly, with decreasing inductance comes increasing inductor discharge rate (as given by (3)), so that less capacitance is needed to ensure regulation during load transients. This is shown in Fig. 1, where the shaded areas under the capacitor current show how the charge that the capacitor needs to handle reduces with increasing frequency. Both factors combine to provide smaller voltage regulation circuitry which is critical for future POL and VRM applications.

A review of commercial POL controller ICs found that switching frequencies of 1 – 4 MHz are supported for current levels up to 6 A when the switches are integrated within the controller IC [7], [8]. Within a given manufacturer, lower frequencies are generally observed for higher current levels and wider input voltage ranges. More recently, the output inductor, L, has been co-packaged with the controller, so that only the output capacitor, C, needs to be added to provide a complete solution [9]. Switching frequencies up to 8 MHz are supported with such solutions. In all cases, the inductor is generally the largest component.

B. Commercial POL Inductor Solutions

In order to benchmark the new core materials proposed, the performance of commercial inductors recommended for POL applications is reviewed. For a typical specification with input voltage range of 2.7 – 5.5 V and an output of 1.8 V at 6 A, the inductance value required to maintain a ripple current ratio of 50% given by (1) is plotted as a function of switching frequency in Fig. 2. Also included are the closest available commercial inductance values that can handle at least 6 A rms and 9 A peak.

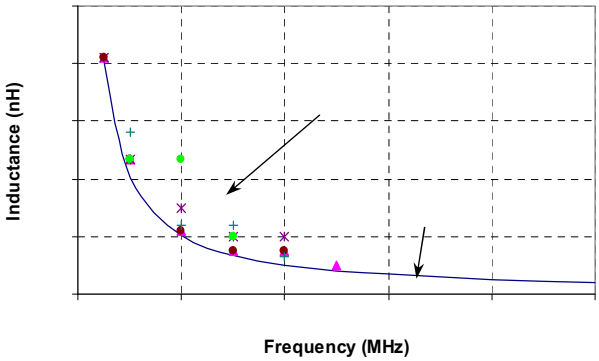

Fig. 2 Inductance vs. frequency for a 6 A POL supply

As given by (1), the inductance value decreases with increasing operating frequency, to give the improvements in steady-state and transient performance described. However, for frequencies greater than 3 MHz, it is seen that the range of commercial inductors available to support such improvements is limited.

Taking 3 MHz as the highest frequency for which commercial inductors are widely available in this case, an inductance of 135 nH is predicted by (1) for the highest input voltage of 5.5 V. The range of compatible commercial devices available from three passive component manufacturers is listed in Table 1, where all components have similar inductance values and maximum current handling levels. It is interesting to note that temperature rise limited current levels more than saturation in all cases.

Table 1: POL inductor specifications

Company	L	I_{max}	Core	Size (mm^3)
Vishay	150 nH	15 A	Powdered iron shielded	6.86 × 6.47 × 1.8
Toko	200 nH	16 A	Powdered iron shielded	7.4 × 6.7 × 3.0
Sumida	150 nH	19 A	MnZn ferrite shielded	10.4 × 10.4 × 5.6

Investigation of the range of core materials used in such inductors revealed that these include metal alloy powder, powdered iron and ferrite. Powdered materials are generally molded to completely enclose helical and sine-shaped coils [10], [11], so that external fringing fields are minimal. Gapped ferrite designs are also usually shielded, although open-cored structures are also applied.

As can be seen, the size of ferrite based designs is generally larger than that of powdered metal designs. This may be explained by losses in the MnZn ferrite applied [12], which is not generally recommended for operation in the MHz range. A review of commercial materials found that only one NiZn grade, 4F1, from Ferroxcube is recommended for frequencies higher than 2 MHz [13]. On the other hand, the powdered core devices in Table 1 are explicitly recommended for operation up to 5 MHz. Again, while no details of losses are provided, it may be expected that core losses limit their application at higher frequencies. This was found in relation to higher current inductors for VRM applications [4] and loss measurements will be performed for the components in

Table 1 under DC/DC switching waveforms to confirm this in the near future.

When the operating frequency is increased to 5 MHz, it is found that only one type of commercial inductor is suitable from the range of manufacturers reviewed. Similarly, if the output current is increased, the range of commercial inductors available to support switching at 1 – 3 MHz is limited. Obviously, this impacts directly on the development of POL solutions for higher current and power levels. The development of electroplated alloy core materials is directed towards addressing this issue.

III. Electroplated Alloy Core Materials

High frequency operation of thin film magnetic alloys is well established in magnetic recording applications, where the frequency range over which magnetic permeability remains constant can be controlled up to the GHz range [14]. For power applications, thick metal alloy tape-wound cores are applied at low frequency, where the thickness of metal layers can be controlled in relation to the skin depth. However, the tape casting process is not suitable for producing metal layers that are sufficiently thin for MHz operation. Electroplating is proposed as a solution in this case.

As the main issue with magnetic materials operating in the MHz range is core loss, the focus of work to date is to identify metal alloy concentrations and plating conditions that provide loss properties competitive to those of available ferrites recommended for MHz operation. In order to identify the most suitable magnetic alloys, the following simple formula was applied to predict the extent to which losses in different alloys can be controlled:

$$P_v = P_{eddy} + P_{hys} = \frac{(\pi f B_{AC} t)^2}{6\rho} + 4 f B_{AC}{}^2 \frac{H_c}{B_{sat}} \qquad (5)$$

where t is the metal layer thickness. In this case, the equation for eddy-current loss, P_{eddy}, is available in the literature [15], while the component of hysteresis loss, P_{hys}, is based on an assumption that the operating value of magnetic field intensity, H, is linearly related to the magnetic flux density, B_{AC}.

Initially, values of material coercivity, H_c, saturation flux density, B_{sat}, and resistivity, ρ, found in the literature were applied in (5). Characteristic measurements were then performed on samples of the most promising materials identified. Results of BH loops produced for two such materials are illustrated in Fig. 3, while results of complex permeability for the same materials are presented in Fig. 4. BH loops were measured using a SHB loop tracer, and a 9 GHz permeameter (model PMM 9G1 from Ryowa) was used to measure complex permeability. Finally, the resistivity of Alloy 1 was measured as 77.8 μΩ-cm with 45 μΩ-cm measured for Alloy 2.

Clearly, when compared with ferrite at ~0.3 T, both alloys have a much higher saturation flux density, with Alloy 2 having the highest value of 1.5 T. The lowest value of coercivity, H_c, measured was 0.2 Oe for Alloy 1. Relative permeability values are also superior to that of 4F1 ferrite, which is constant at 80 up to 30 MHz [13].

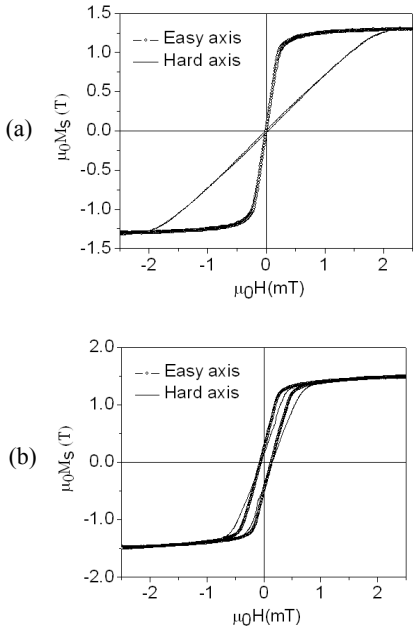

Fig. 3 BH loops of (a) Alloy 1 and (b) Alloy 2

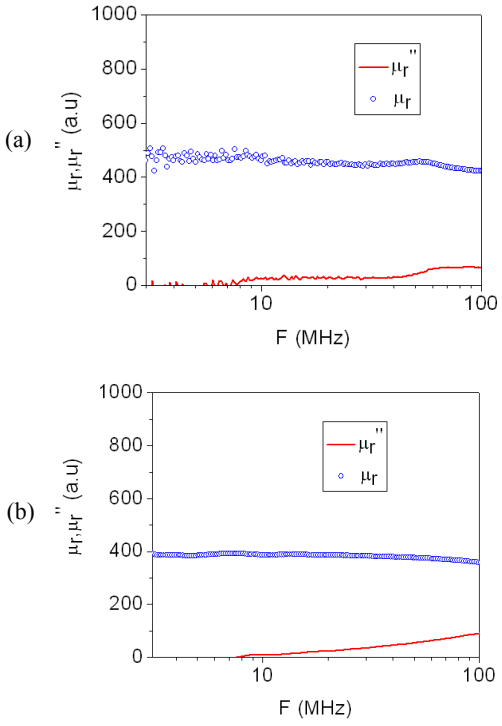

Fig. 4 Complex permeability of (a) Alloy 1 and (b) Alloy 2

These values were applied in (5) to calculate power loss density, P_v, for the materials for comparison with measured losses; results are presented in Fig. 5 at 3 and 5 MHz. Values quoted by Ferroxcube for 4F1 are included for comparison. When compared to previous samples which had only 4 layers of magnetic material [4], the samples used in Fig. 5 have approximately 30 layers of metal alloy ribbon rolled into a ring core. The materials were plated onto 6 μm thick insulation and an additional adhesive tape was used to provide mechanical strength.

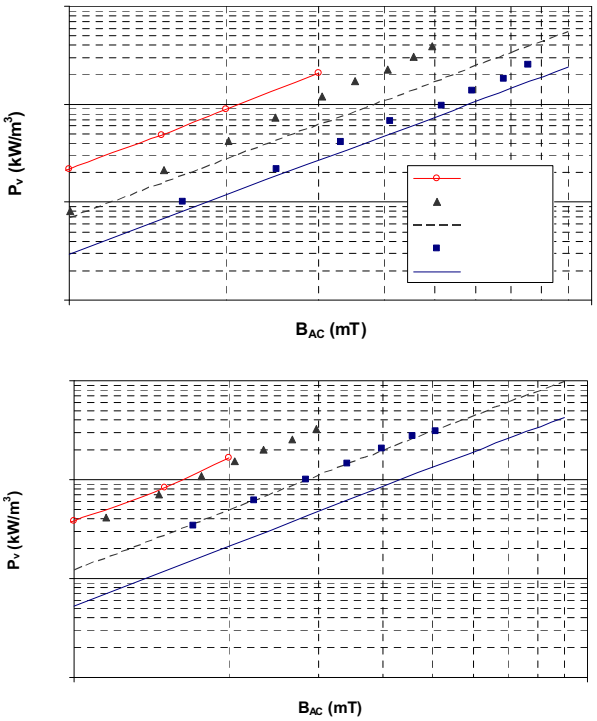

Fig. 5 Power loss density, P_v, vs. B_{ac} for metal alloys at (a) 3 MHz and (b) 5 MHz

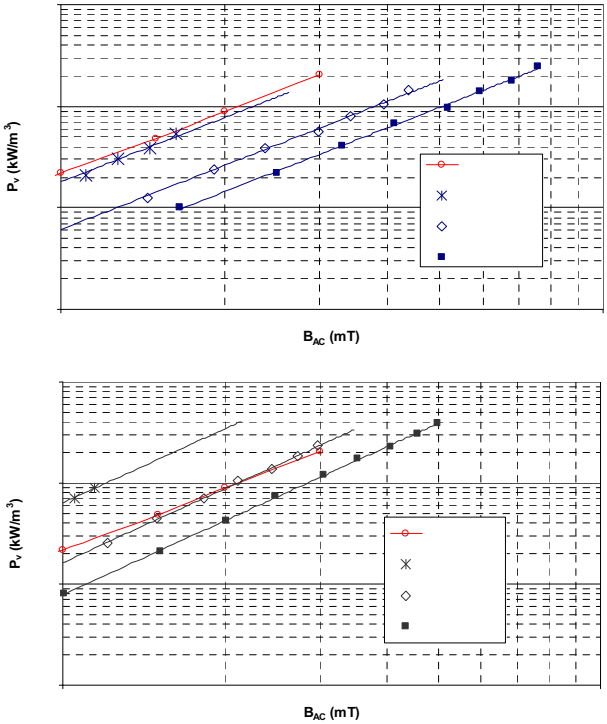

Fig. 6 Average power loss density vs average B_{AC} for (a) Alloy 1 and (b) Alloy 2

Loss measurements were carried out using the transformer method [16], with compensation included for the delay of the current probe and air-core leakage effects. As shown, both materials provide improved loss properties compared to 4F1 up to 5 MHz, with Alloy 1 providing the best performance. Agreement between models and measurements is better at the lower frequency and this may be explained by fringing effects between neighbouring metal layers, because the thickness of insulation is relatively thick compared to the thickness of metal. Measurements on the same samples with different wound configurations will be performed to investigate this effect more closely.

In terms of inductor design, (1) can be written in terms of the inductor structure as:

$$D(V_{in} - V_o) = fNA_c\Delta B \qquad (6)$$

Where N is the number of winding turns and A_c is the core area. Clearly, higher allowed levels of magnetic flux density excitation, $B_{AC} = \Delta B/2$, translate into correspondingly smaller values of NA_c and therefore inductor size. In Fig. 5 it is seen that if the power loss density of the core materials is limited to a certain value (to limit temperature rise), a larger value of flux excitation is allowed for the metal alloys than for ferrite. However, from a practical point of view, a layer of insulation must be inserted between each pair of foil layers, and therefore the factor of reduction in size is lower than predicted from Fig. 5 directly. In order to investigate this effect further, results of power loss and magnetic flux density measured in Fig. 5 are averaged over the total core volume and total core area respectively, for two different values of insulation thickness, ti, in Fig. 6.

Obviously, the thinner insulation provides the best results for both materials. As in Fig. 5, the performance of Alloy 1 is better than that of Alloy 2, with the allowed magnetic flux density excitation level being 1.8 times larger than that of ferrite at a power loss density value of 500 kW/m^3. Samples to date have been produced on 6 μm thick insulation and work is ongoing to develop plating processes for thinner layers.

IV. Electroplated Alloy Core Design

The potential improvement in size of POL inductors offered by the use of laminated metal alloy cores is illustrated in this section for the materials described in section III. For simplicity, a single-turned bead inductor structure is assumed, having the geometrical parameters shown in Fig. 7. The first step in design is to choose a winding area that is large enough to handle the rms current level to be applied. In order to limit current density to the AWG limit of 2 A/mm^2 a copper strap with cross section, $w_{Cu} \times h_{Cu} = 3.25 \times 0.127$ mm^2 was chosen as suitable for rms current levels up to 9 A.

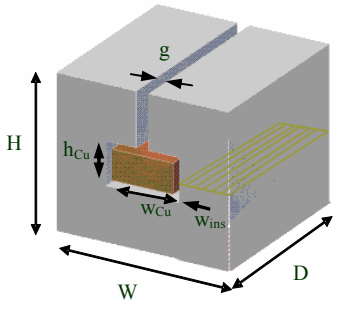

Fig. 7 Bead inductor structure

The next step is to determine the minimum core area, A_c, required to prevent excessive core loss using (6) with N set equal to 1:

$$Ac = \frac{D(V_{in} - V_o)}{2fB_{AC\,max}} \quad (7)$$

Here, $B_{AC\ max}$ is the magnetic flux density for which the power loss density, P_v, of the core material is 500 kW/m^3. As described in relation to Fig. 6, $B_{AC\ max}$ and P_v should be averaged over the total volume and area of the core. The resulting core area is applied to define a bead inductor with a square footprint, W × D, as shown in Fig. 7. The last step is to calculate the gap required to limit inductance, L, as this is found to be larger than that needed to prevent saturation for MHz operation. With l_c calculated as the average magnetic path length through the core:

$$L = \frac{\mu_o A_c}{g + l_c / \mu_r} \quad (8)$$

Based on the results of Fig. 6, details of designs produced following the above procedure are given for Alloy 1 and Alloy 2 with 1 μm insulation in Table 2. The same procedure was applied for 4F1 ferrite for comparison.

Table 2 POL inductor designs

Frequency	Core material	Gap (μm)	Size (mm^3) W × D × H
3 MHz	4F1	None	8.9 × 8.9 × 5.8
	Alloy 1	21.1	5.8 × 5.8 × 2.7
	Alloy 2	58.3	7.0 × 7.0 × 3.9
5 MHz	4F1	None	6.7 × 6.7 × 3.6
	Alloy 1	75.7	6.0 × 6.0 × 2.9
	Alloy 2	138.0	7.0 × 7.0 × 3.9

Clearly, the size of designs with electroplated alloy cores is smaller than those produced with 4F1 at 3 MHz, with the footprint of the Alloy 1 design being only 42% that of 4F1. When compared with the size of commercial components in Table 1, Alloy 1 is also shown to be competitive to powdered metal materials, with Alloy 2 being less so. Due to the higher rate of increase in loss with frequency for the alloys, the size of corresponding cores at 5 MHz is larger than at 3 MHz. However, as losses are most likely due to excessive fringing in the applied samples, smaller components may be expected if an insulation thickness of 1 μm can be realised.

It is interesting to note that the core area of the ferrite inductor needed to be increased over that calculated by (7) in order to achieve the inductance value required. This is explained by its relatively low permeability of 80, when compared to that of the alloys. By comparison, it was necessary to include a gap in the design of all alloy cores, as the inductance provided by the core area of (7) was too large.

The relative contributions of DC winding loss, P_{Cu}, and sinusoidal core loss, P_{core}, are compared for the different solutions at 3 MHz in Fig. 8. The dominance of core loss is obvious in all designs. Highest losses are seen for the design based on Alloy 2 at both frequencies and this is explained by higher core loss characteristics. As no account was taken of eddy-current effects in the windings or of non-sinusoidal waveform effects on core losses, the

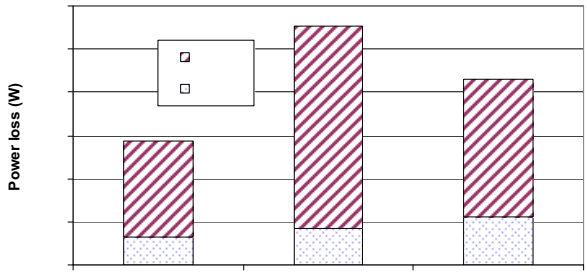

Fig. 8 POL inductor losses at 3 MHz

difference between results at 3 MHz and 5 MHz is not significant. Work is ongoing to investigate these additional contributions to total loss.

V. Inductor Measurements

The rolled sample of Alloy 1 was applied to produce a 100 nH inductor for operation at 3 MHz, to illustrate the application of the material under DC/DC switching waveforms. Results of inductance vs. frequency for the device are given in Fig. 9.

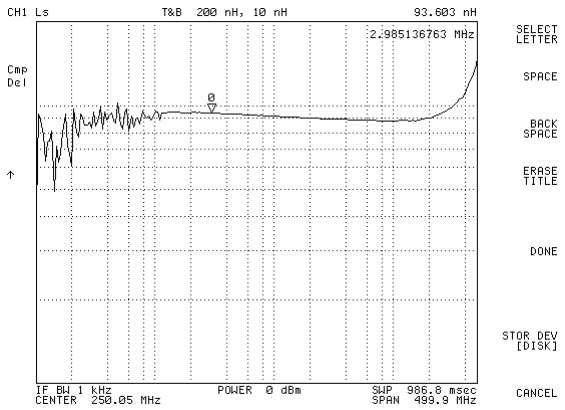

Fig. 9 Measured inductance vs. frequency for test inductor

The performance of the material operating under DC/DC switching waveforms was measured for a range of output current levels using a 3 MHz test VRM circuit as shown in Fig. 10. The circuit was designed for output current levels up to 30 A and for switching frequencies up to 3 MHz. In this case, the maximum output current was limited to 6 A., for which plots of voltage and current waveforms for the inductor are shown in Fig. 11.

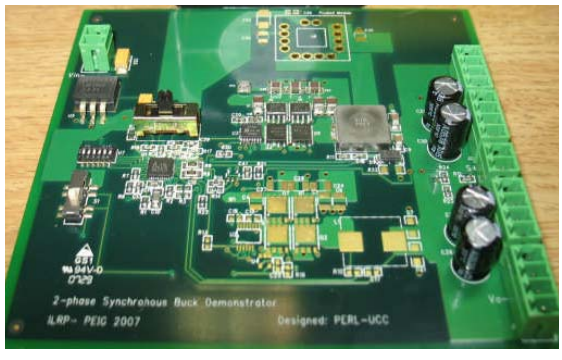

Fig. 10 Photograph of test POL circuit

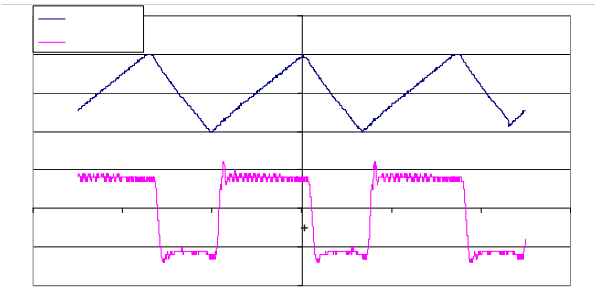

Fig. 11 Inductor voltage and current waveforms under 3 MHz DC/DC excitation

From the applied voltage and current levels, the inductance value is calculated to be 84 nH and this remained practically constant for all current levels. The corresponding levels of magnetic flux density are estimated as 300 mT DC and 200 mT AC. In this case, the size of the inductor is dominated by the large thickness of insulation used to provide mechanical support for the material. However, with a manufacturing process capable of winding ribbons of the material with thinner insulation, the size of the inductor could be reduced to that predicted in section IV. The authors are contacting a number of component manufacturers with a view to developing such a process.

VI. Conclusions

The application of electroplated alloys in magnetic core solutions for point-of-load inductors is investigated at frequencies up to 5 MHz, where the alloy loss properties are shown to be competitive to the best ferrite materials available. Measured results of power loss density are provided for bulk-type material samples of two alloys. When applied to the design of bead inductors, the size of the resulting devices is reduced to 42% that of the comparable design based on 4F1, and to 76% of typical commercial devices.

The next step in the work is to provide a manufacturing process that will support thin layers of insulation required to prevent shorting between neighbouring metal layers. Collaboration with commercial manufacturers will be developed to facilitate this.

Acknowledgments

This work has been funded by Enterprise Ireland, the National Development Plan and the European Union under the Industry Led Research Programme in Power Electronics and by Science Foundation Ireland (SFI).

References

[1] R. Huljak, V. Thottuvelil, A. Marsh, B. Miller; '*Where are power supplies headed?*', Proceedings of APEC 2000, Vol. 1, pp. 10-17.

[2] L. Daniel, C. Sullivan, S. Sanders; '*Design of microfabricated inductors*', IEEE Transactions on Power Electronics, Volume 14, Issue 4, July 1999, pp. 709 – 723.

[3] S. Prabhakaran, C. Sullivan, T. O'Donnell, M. Brunet, S, Roy; '*Microfabricated coupled inductors for DC/DC converters for microprocessor power delivery*', Proceedings of PESC 2004, pp. 4467 – 4472.

[4] S. Kelly, C. Collins, M. Duffy, F. M. F. Rhen, S. Roy; '*Core materials for high frequency VRM inductors*', Proceedings of PESC 2007, pp. 1767 – 1772.

[5] ISL6307 6-phase PWM controller datasheet, Intersil, www.intersil.com

[6] Type 59P datasheet, '*SMD high frequency power inductors*', Vitec Corporation, www.viteccorp.com

[7] MAX1945 datasheet, Maxim, www.maxim-ic.com

[8] MIC22400 datasheet, Micrel, www.micrel.com

[9] D. Morrison, '*Regulators embed inductors to save space and ease use*', Power Electronics Technology, July, 2007.

[10] T. Shafer, '*Inductor coil structure*', US Patent No. 6,198,375, 6th March, 2001.

[11] T. Shafer, '*High current, low profile* inductor', US Patent No. 6,204,744, 6, 20th March 2001.

[12] CDEP105 datasheet, Sumida Corporation, www.sumida.com

[13] www.ferroxcube.com

[14] S.H. Kong, T. Okamoto, S. Nakagawa; **'***Fe-Co-B/Ni-Fe soft magnetic underlayer with high-saturation magnetization for perpendicular magnetic recording media'*, IEEE Transactions on Magnetics, Volume 39, Issue 5, Part 2, Sept. 2003, pp. 2285 – 2287.

[15] E. C. Snelling, '*Soft ferrites, properties and applications*', Butterworths, 2nd edition, 1988

[16] N. Schmidt and H. Guldner, 'A simple method to determine dynamic hysteresis loops of soft magnetic materials', IEEE Trans.Magn. 32, 489 (1996).